

Gel-polymer Electrolytes based on Poly(ionic liquid)/ionic liquid Networks

Sudeshna Sen,^a Sean E. Goodwin,^a Pedro Verdía Barbará,^a Graham A. Rance,^{a,b} Dominic Wales,^{c,§}

Jamie M. Cameron,^a Victor Sans,^c Mohamed Mamlouk,^d Keith Scott,^d and Darren A. Walsh^{a*}

^a Nottingham Applied Materials and Interfaces (NAMI) Group, School of Chemistry and GSK

Carbon Neutral Laboratories for Sustainable Chemistry

The University of Nottingham, Jubilee Campus

Nottingham NG7 2TU, UK

^b Nanoscale and Microscale Research Centre (nmRC)

The University of Nottingham, University Park Campus

Nottingham NG7 2RD, UK

^c Faculty of Engineering and GSK Carbon Neutral Laboratory for Sustainable Chemistry

The University of Nottingham, Jubilee Campus

Nottingham NG7 2TU, UK

^d School of Engineering, Merz Court,

Newcastle University

Newcastle-upon-Tyne NE1 7RU, UK

§ Present address: Hamlyn Centre, Faculty of Engineering, Imperial College London, South

Kensington Campus, London, SW7 2AZ, UK

[*darren.walsh@nottingham.ac.uk](mailto:darren.walsh@nottingham.ac.uk);

Tel: +44 115 846 7495; Fax: +44 115 951 3462

ABSTRACT

The use of electrically-charged, polymerized ionic liquids (polyILs) offers opportunities for the development of gel-polymer electrolytes (GPEs), but the rational design of such systems is in its infancy. In this work, we compare the properties of polyIL/IL GPEs based on 1-butyl-3-(4-vinylbenzyl)imidazolium bis(trifluoromethanesulfonyl)imide containing trapped ammonium-based protic ionic liquids (ILs) with an analogous series based on the electrically-neutral host polymer 1-(4-vinylbenzyl)imidazole. The materials are synthesised by photopolymerising ionic and neutral monomers in the presence of diethylmethylammonium trifluoromethanesulfonate, [dema][TfO], diethylmethylammonium trifluoroacetate, [dema][TFAc], and diethylmethylammonium bis[trifluoromethanesulfonyl]imide, [dema][Tf₂N], respectively. The resulting materials are characterized using electron microscopy, infra-red spectroscopy, thermal analysis, Raman spectroscopy, and AC-impedance analysis. Spectroscopic analysis confirms that the ILs are distributed throughout the polymers, unless the GPE also contains poly(diallyldimethylammonium bis[trifluoromethanesulfonyl]imide), when separation of the components occurs. The polyIL/IL GPEs are more electrochemically and thermally stable, and up to 6 times more conductive, than the materials based on the neutral host. As a proof-of-concept demonstration, we show that polyIL/IL gels can be 3-D printed using readily available 3D-printing hardware.

Keywords: conductivity; polymer electrolytes; membranes; photopolymerization; ionic liquids; poly(ionic liquid)

INTRODUCTION

Ionic liquids (ILs) are salts that are liquid below 100 °C and which, due to their inherent conductivity, wide potential windows, low volatility, and thermal stability, are being used in a range of applications, including separations,¹ sensing,² energy conversion,³ biocatalysis,⁴ and photochemistry.⁵ In many of these applications, the use of solid or semi-solid ionic materials is preferable, due to the simplicity of device construction and operational safety. Consequently, the use of gel-polymer electrolytes (GPEs) in which ILs are trapped within polymeric hosts has emerged in recent years.⁶ These “ion gels” have been used in electronic,⁷ microfluidic,⁸ and electrochemical devices⁹ and have been synthesized by (i) swelling pre-formed polymers in ILs,¹⁰ (ii) co-dissolving polymers and ILs in a solvent that is subsequently removed,¹¹ and (iii) polymerizing monomers in the presence of ILs.¹²

A particular advantage of IL-based GPEs is the high thermal stabilities of the membranes that can be obtained. For example, Xie and co-workers incorporated the IL N-methyl-N-butylpiperidine difluoromethylimide into poly(vinylidene fluoride-co-hexafluoropropylene) membranes to make GPEs for Na-ion batteries that were thermally stable to 450 °C.¹³ Zheng and co-workers formed poly(vinyl alcohol)-based membranes containing ammonium-based ionic liquids for use as proton exchange membranes, which were stable up to 160 °C, considerably higher than that achievable using conventional membranes (~80 °C).¹⁴ Langevin and co-workers synthesized proton-conductive GPEs that could operate at 130 °C, by incorporating triethylmethylammonium trifluoromethanesulfonate into polyimide membranes.¹⁵

As well as trapping ILs in “conventional” polymers, IL-based GPEs have been formed by trapping ILs in polymerized ionic liquids (polyILs), with the aim of exploiting potential

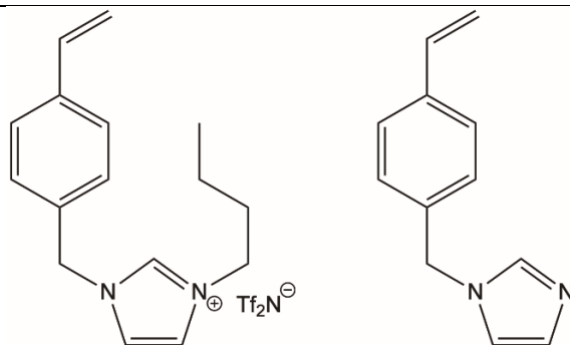
compatibility between the ILs and the polyIL hosts.^{16,17} As they are also ionic materials, polyILs are inherently chemically and thermally stable and ionically conductive, and their physicochemical properties can be precisely tuned by changing their ionic composition. For example, the presence of aromatic groups in the polymer structure can enhance its thermal stability. In terms of the ionic composition, the thermal stability of polyILs generally decreases in the order imidazolium > pyridinium > pyrrolidinium > ammonium for common polyIL cations and bis(trifluoromethanesulfonyl)imide ([Tf₂N]⁻) > [CF₃SO₃]⁻ > [BF₄]⁻ > [PF₆]⁻ > [Br]⁻ for common polyIL anions.¹⁸ PolyILs have been formed by polymerizing pendant groups on the cations and anions of polymerizable ILs¹⁹ and used in several applications. PolyIL/IL GPEs based on poly(diallyldimethylammonium) bis(trifluoromethanesulfonyl)imide, [PDADMA][Tf₂N], and a range of crosslinkers, plasticizer ILs, and dopants, have been synthesized and used to construct non-flammable Li-ion batteries.²⁰ Physical or chemical cross-linking of the polymeric backbone has also been used to mitigate against exclusion of the free IL component from the polymer and enhance the thermal stability of the GPE.²¹

As polyIL/IL GPEs are being used as electrolytes for devices such as Li-ion batteries²² and fuel cells,^{23,24} the effects of GPE composition on ionic conductivity are often a primary concern during development of these materials. Conductivities in the range 10⁻⁴-10⁻³ S cm⁻¹ have been reported for polyIL/IL GPEs, and can be tuned by changing the composition of the polyIL and/or IL.²⁵ For example, Odriozola and co-workers added pendant poly(ethylene glycol) (PEG) side chains to pyrrolidinium-based polyILs, increasing the conductivity over that of the unmodified material.²⁶ Dicationic polyIL crosslinkers have been added to poly(1-[2-(acryloyloxy)ethyl]-3-ethylimidazolium bis(trifluoromethanesulfonyl)imide) containing the ILs 1-ethy-3-

methylimidazolium bis(trifluoromethanesulfonyl)imide and 1-ethyl-3-methylimidazolium tetrafluoroborate, yielding membranes with a conductivity of $3.63 \times 10^{-3} \text{ S cm}^{-1}$ at $50 \text{ }^\circ\text{C}$.²⁷ An interesting factor in the development of polyIL/IL GPEs is the effect of the charge on the polyIL backbone on the properties of the resulting material. Yan and co-workers compared the conductivity of a GPE based on dicationic 1-butyl-3-(1-vinylimidazolium-3-hexyl)imidazolium bis(trifluoromethanesulfonyl)imide) monomers with one based on monocationic 1-butyl-3-(1-vinyl)imidazolium bis(trifluoromethanesulfonyl)imide) monomers, and each was combined with a mixture of 1-ethyl-3-methylimidazolium iodide, 1-propyl-3-methylimidazolium iodide, and 1-ethyl-3-methylimidazolium thiocyanate. The material based on the monocationic monomers exhibited a conductivity of $2.92 \times 10^{-3} \text{ S cm}^{-1}$, while that of the material based on the dicationic monomers was $5.83 \times 10^{-3} \text{ S cm}^{-1}$.²⁸

In this contribution, we describe a class of GPEs formed by polymerizing 1-butyl-3-(4-vinylbenzyl)imidazolium] bis(trifluoromethanesulfonyl)imide, [BVBIIm][Tf₂N] (Scheme 1 left), which was specifically chosen due to the thermal stability of this combination of ionic components. The GPEs are formed by polymerizing the ionic monomers in the presence of the ILs diethylmethylammonium trifluoromethanesulfonate, [dema][TfO], diethylmethylammonium trifluoroacetate, [dema][TFAc], and diethylmethylammonium bis[trifluoromethanesulfonyl]imide, [dema][Tf₂N], respectively. These ammonium-based ILs represent a class of proton-conductive electrolytes that have been used as electrolytes in intermediate-temperature ($>100 \text{ }^\circ\text{C}$) H₂ fuel cells under conditions of very low humidity.^{29,30} Protic ionic liquids have been entrapped within neutral polymers such as polybenzimidazole and sulfonated polyimides for such devices previously.^{31,32,33} Our aim was to explore the opportunities

offered by polyIL-based host polymers for such functional systems by combining the thermally-stable [BVBIIm][Tf₂N] host with the proton-conductive, ammonium-based protic liquids. Furthermore, we set out to compare the physicochemical properties of these materials with a class in which the host polymer is electrically neutral, to explore complementarity between the polyILs and liquid IL components in such systems. The polyIL/IL GPEs were formed by trapping the protic ionic liquids during photopolymerization of [BVBIIm][Tf₂N], using 1,4-butanediol diacrylate (BDA) and diphenyl(2,4,6-trimethylbenzoyl)phosphine oxide as cross-linker and photoinitiator, respectively.³⁴ The GPEs based on the neutral polymer host was formed by polymerizing the uncharged, but structurally-similar, 1-(4-vinylbenzyl)imidazole (which we label Im, Scheme 1 right), meaning that the primary difference between our classes of GPEs was the charge on the polymer-host backbone (rather than any structural differences). The conductivities of the polyIL/IL membranes are up to 6 times higher than those of the GPEs based on the neutral host. We show that incorporating a second polyIL into the polyIL/IL GPE can affect the spatial distribution of the trapped IL, but with no effect on the GPE conductivity. Finally, and as a proof-of-concept demonstration, we show that GPEs based on [dema][TfO] trapped within poly([BVBIIm][Tf₂N]) can be 3D printed using readily available printing technology.



Scheme 1. Chemical structure of (left) 1-butyl-3-(4-vinylbenzyl)imidazolium bis(trifluoromethanesulfonyl)imide, which is denoted [BVBI_m][Tf₂N], and (right) 1-(4-vinylbenzyl)imidazole, which is denoted Im.

EXPERIMENTAL SECTION

Reagents and Apparatus. Reagents were obtained from Sigma-Aldrich or Alfa Aesar and were used as received. Poly(diallyldimethylammonium) chloride (average MW 400,000–500,000, 20 wt.% in H₂O) was used as received. 1,4-butanediol diacrylate and divinylbenzene were passed through an activated basic alumina column 3 times prior to use.

Attenuated total reflectance, Fourier-transform infrared (FTIR) spectra were recorded using a Perkin Elmer Spectrum 2000 spectrometer, at a spectral resolution of 4 cm⁻¹. All measurements were carried out at ambient temperature and in the range 400–4000 cm⁻¹. Nuclear magnetic resonance (NMR) spectra were acquired using a Bruker AVIII 400 spectrometer, with d₆-dimethylsulfoxide and trimethylsilane as the solvent and reference, respectively. Mass-spectrometry samples were dissolved in dry acetonitrile to a concentration of 10⁻⁶ mol dm⁻³ and were analysed using Bruker MicroTOF spectrometer and electrospray ionisation. Thermogravimetric analysis was carried out using Pt pans under N₂ using a TA Instruments Discovery Thermogravimetric Analyser (Discovery TGA) at a heating rate of 10 °C min⁻¹. Karl-Fischer titrations were performed using a CA200 moisturemeter (Mitsubishi Chemical Analytech). Differential scanning calorimetry was carried out using TA instruments Tzero aluminum pans with Tzero Hermetic Lids on a TA Instruments Discovery differential scanning calorimeter. The loading of ILs in the membranes was determined gravimetrically by measuring the mass lost after immersion in H₂O for 72 h (replacing the H₂O every 24 h) and drying at 60 °C for 24 h.

Conductivities, σ , were measured using AC-impedance spectroscopy (CH Instruments Model 760D) in the frequency range 1-10⁵ Hz, and were calculated using the equation $\sigma = L/RA$, where L is the distance between two electrodes or sample thickness for solid films, A is the area of the electrodes, and R is the sample resistance. R was determined from the high frequency impedance intercept on the x -axis of Nyquist plots (Z' vs $-Z''$). GPE membranes were cut into 12 mm \times 12 mm squares with thicknesses ranging from 200-400 μm . The solid films were sandwiched between 1 cm² Pt-plate electrodes. Conductivities of liquid samples were analysed using a conductivity cell containing two Ag-rod electrodes. The cell constant was determined using a 1.0 mol dm⁻³ NaCl standard solution. Variable-temperature measurements were performed by immersing the conductivity cell into a temperature-controlled silicone-oil bath. All measurements were performed in the range 40-190 °C, in intervals of 15 °C.

Scanning electron microscopy (SEM) was carried out using a Zeiss EVO10 spectrometer. Micro-Raman spectroscopy was performed using a Horiba Jobin Yvon LabRAM HR Raman spectrometer, equipped with an automated xyz stage (Märzhäuser). Spectra were acquired using a 785-nm laser (running at 25 mW), a 100 \times objective lens, and a 50- μm confocal pinhole. To simultaneously scan a range of Raman shifts, a 600-lines mm⁻¹ rotatable diffraction grating along a path length of 800 mm was used. Spectra were acquired using a Synapse CCD detector (1024 pixels), thermoelectrically cooled to -60 °C. Before collection of spectra, the instrument was calibrated using the zero-order line and a standard Si(100) reference band at 520.7 cm⁻¹. For single point measurements, spectra were acquired in the range 150-4000 cm⁻¹ (8 spectral windows), using 2-4 accumulations with an acquisition time of 15-60 seconds. The spectral resolution in this configuration is better than 0.8 cm⁻¹. Spectra were baseline-corrected using a fourth-order

polynomial subtraction. Lateral (x-y) spectroscopic maps of the surfaces of the films were obtained in the range 150-2000 cm^{-1} (3 spectral windows) at 5- or 10- μm steps within an area of $225 \times 225 \mu\text{m}$ (a total of 2116 or 576 spectra, respectively). The DuoScan functionality was employed to confer a spatial resolution of $5 \times 5 \times 5 \mu\text{m}$ or $10 \times 10 \times 5 \mu\text{m}$ (*xyz*), respectively. Axial (*z*) spectroscopic maps were obtained in the range 150-2000 cm^{-1} (3 spectral windows) in 5- μm steps at depths of 0-50 μm . The intensity of diagnostic vibrational modes of polymers and ILs were evaluated within each map using either univariate or multivariate analysis (as classic least-squares regression analysis) within Labspec 6.4.3. software.

Synthesis of Protic ILs. [dema][TfO], [dema][TFAc], and [dema][Tf₂N] were synthesized by neutralising N,N-diethylmethylamine (dema) with the corresponding Brønsted acids.³⁵ Aqueous 1.0 mol dm^{-3} solutions of the appropriate acids (trifluoromethanesulfonic acid, HTfO, trifluoroacetic acid, HTFAc, and hydrogen bis(trifluoromethane)sulfonamide, HTf₂N) were added dropwise to 1.05 mol equivalent of dema (kept in an ice bath) and stirred for 1 hr. Excess water and dema were removed using rotary evaporation and, prior to use, the liquids were dried under vacuum at 70 °C for 72 hr. Residual water contents were measured using Karl-Fischer titrations and were 30 ppm, 21 ppm and 32 ppm for [dema][TfO], [dema][TFAc], and [dema][Tf₂N], respectively.

Synthesis of GPE Membranes. Detailed descriptions of the synthesis of GPEs are in the supporting information. Briefly, appropriate quantities of monomers, ILs, 1,4-butanediol diacrylate (BDA), photoinitiator, and copolymer were stirred in the dark for 1 hr. Solutions were then sandwiched between two glass plates and polymerised for 1 hr using a UV lamp (365 nm/36W) held 5 cm from the solutions (Figure S2). The GPEs made by incorporating [dema][TfO],

[dema][TFAc], and [dema][Tf₂N] into the polyIL membranes are denoted polyIL/[dema][TfO], polyIL/[dema][TFAc], and polyIL/[dema][Tf₂N], respectively. GPEs made by incorporating the ILs into poly[1-(4-vinylbenzyl)imidazole] are denoted polyIm/[dema][TfO], polyIm/[dema][TFAc], and polyIm/[dema][Tf₂N]. A [BVBIIm][Tf₂N]/[dema][TfO] GPE containing the polyIL polydiallyldimethylammonium bis(trifluoromethanesulfonyl)imide, [PDADMA][Tf₂N], was formed by adding 5 wt.% of [PDADMA][Tf₂N] to the reaction mixture. This GPE is denoted polyIL/[PDADMA][Tf₂N]/[dema][TfO]. A summary of the compositions of the materials investigated in this work is given in Table S1.

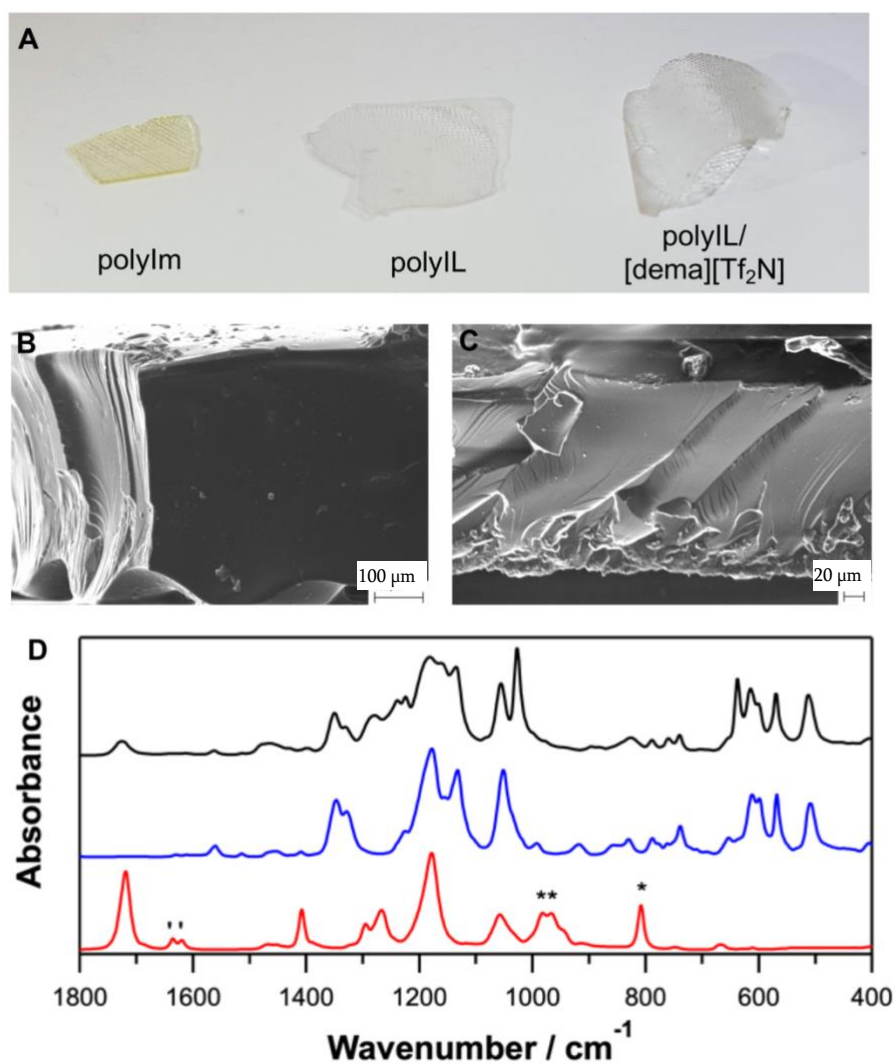


Figure 1. (A) Photographs of $\sim 1\text{cm}^2$ samples of various membranes. (B) SEM image of the polyIL/[dema][TFAc] membrane. (C) SEM image of the polyIm/[dema][TfO] membrane. (D) FTIR spectra of polyIL/[dema][TfO] (black), the [BVBIIm][Tf₂N] monomer (blue), and the BDA cross-linker (red).

RESULTS AND DISCUSSION

The films formed by polymerizing Im and [BVBIIm][Tf₂N] were free-standing and uniform (Figure 1A) and SEM showed that the GPE surfaces and cross sections (Figures 1B and C) were smooth. The FTIR spectrum of the BDA cross-linker (red line in Figure 1D) contains various peaks that disappeared after polymerisation, including those at 1619 and 1636 cm^{-1} due to stretching of the C=C functional group of the terminal vinyl ester moieties (labelled ν),³⁶ and peaks at 966, 983 and 807 cm^{-1} (labelled \ast) which are characteristic of a vinyl group coupled with a carbonyl group.³⁷ The strong signal due to stretching of the C=O bond of the α,β -unsaturated ester group of BDA shifted from 1718 to 1724 cm^{-1} after polymerisation. The spectrum of [VBBIm][Tf₂N] (blue line in Figure 1D) also contains various peaks that disappeared after polymerisation, such as the bands at 919 and 993 cm^{-1} , which are also characteristic of vinyl groups.³⁷ The FTIR spectra of [VBBIm][Tf₂N] and polyIL/[dema][TfO] have a number of features consistent with the presence of the [Tf₂N]⁻ anions, such as those in the region 500-600 cm^{-1} .^{38,39,40} The presence of [dema][TfO] in the GPE is also confirmed by the appearance of peaks not present in the spectra of BDA or the [BVBIIm][Tf₂N] monomers, such as the peaks at 1026 cm^{-1} , which is attributed to the stretching of

the C-F bonds in the [TfO]⁻ anions,⁴¹ and at 1280 cm⁻¹, due to the stretching of the N-H bonds of the [dema]⁺ cations.⁴²

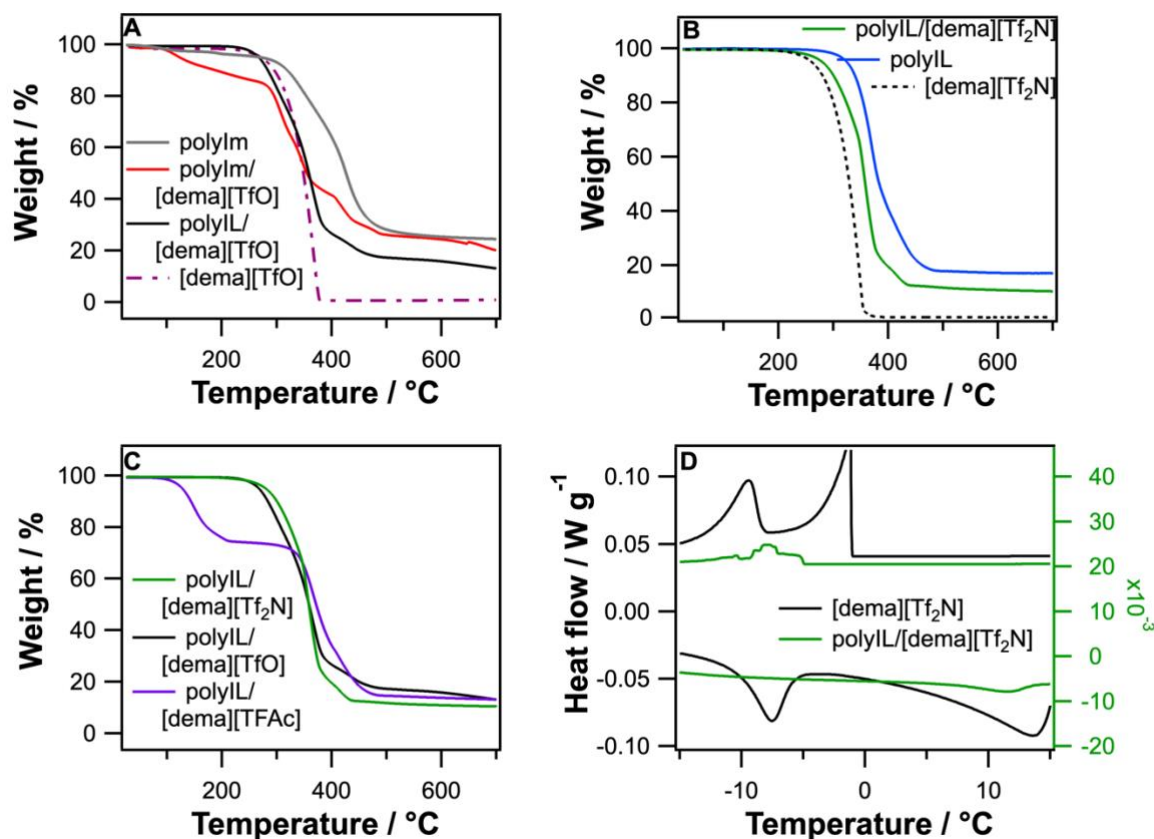
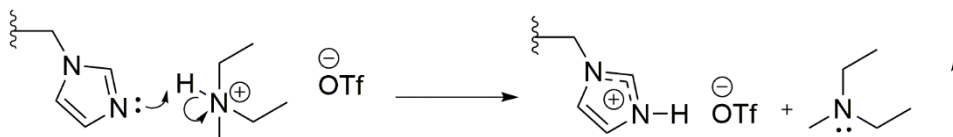


Figure 2. (A-C) TGA traces of various materials, recorded using a heating ramp of 5 °C min⁻¹ between 25 °C and 700 °C. (D) DSC traces of polyIL/[dema][Tf₂N] and free [dema][Tf₂N].

The thermal stability of the materials was examined using thermogravimetric analysis (TGA) under N₂ (Figure 2A-C). The temperatures at which 1% and 10% of the initial weight were lost ($T_{1\%}$ and $T_{10\%}$) and the peak weight-loss temperature (T_{peak}) were determined as comparators. Table 1 shows that T_{peak} of the undoped polyIL was 367.7 °C, while that of undoped polyIm was 428.6 °C. By 400 °C, the polyIL membrane retained 40.7% of its original mass compared to 64.1%

for polyIm (Figure 2A and 2B). The polyIm and doped polyIm/[dema][TfO] membranes both lost weight upon initiation of heating; $T_{1\%}$ of polyIm was 71.8 °C, and 3.7% mass was lost by 200 °C (Figure 2A). Remarkably, incorporating [dema][TfO] into polyIm decreased its thermal stability; $T_{1\%}$ of polyIm/[dema][TfO] was 36.1 °C, and the mass loss at 200 °C was 10.8 %. A potential explanation for this effect is protonation of the imidazole ring of the polymer by the IL cations, releasing volatile dema (Scheme 2) To test this possibility, diethyldimethylammonium trifluoromethanesulfonate, [dedma][TfO], which is structurally similar to [dema][TfO] but cannot donate protons to the polymer, was used as the dopant (Table 1, 7th entry). The resulting GPE was more stable than polyIm/[dema][TfO], supporting the possibility that the mechanism in Scheme 2 could have resulted in decomposition of polyIm/[dema][TfO]. However, we do note that the pK_a (in aqueous media) of the [dema]⁺ cation (*ca.* 10) is higher than that of the imidazole group (*ca.* 7), which might suggest that such an explanation is unlikely.⁴³ On the other hand, several studies have shown that pK_a values diverge significantly on moving from aqueous to ionic liquid media,⁴⁴ while it is known that increasing the temperature has significant effects pK_a values. It is also interesting to note that T_{peak} of polyIL/[dema][Tf₂N] was lower than for the undoped polyIL, which cannot have been due to the reaction in Scheme 2, as there are no proton acceptor sites on the polyIL membranes. It appears that decomposition of polyIL/[dema][Tf₂N] occurs first by decomposition of [dema][Tf₂N], which is less thermally stable than the host polyIL (Figure 2B). Clearly these data show that more work is required to understand the thermal decomposition of these materials completely, but the general thermal stability of the polyIL/IL materials offers prospects for the future development of intermediate-temperature devices using these systems.



Scheme 2. Possible mechanism for the thermal decomposition of polyIm/[dema][TfO].

Table 1. Thermogravimetric data for various GPEs.

Material	$T_{1\%} / ^\circ\text{C}$	$T_{10\%} / ^\circ\text{C}$	$T_{\text{peak}} / ^\circ\text{C}$
polyIm	71.8	318.8	428.6
polyIL	278	339.3	367.7
[dema][TfO]	30.6	295.0	371.2
[dema][TFAc]	84.6	143.2	373.6
[dema][Tf ₂ N]	204.7	280.4	349.8
polyIm/[dema][TfO]	36.1	187.7	345.1
polyIm/[dedma][TfO]	137.7	283.7	398.4
polyIL/[dema][TfO]	222	283.5	367.6
polyIL/[dema][TFAc]	84.6	143.2	373.6
polyIL/[dema][Tf ₂ N]	208	299.7	356.8
polyIL/[PDADMA][Tf ₂ N]	215.5	296.4	377.1
/[dema][TfO]			

Figure 2C shows TGA curves for polyIL/[dema][TfO], polyIL/[dema][TFAc] and polyIL/[dema][Tf₂N] and reveals considerable differences in their thermal stability. Using $T_{10\%}$ as a comparator, the stability of the IL doped membranes decreased with the anion type in the order [TFAc]⁻ < [TfO]⁻ < [Tf₂N]⁻, which is the inverse of the order of proton affinity of the acids used to generate the ionic liquids.⁴⁵ Weaker acids have a higher proton affinity, resulting in a weaker bond between the proton of the precursor acids and the amine of the base. This indicates that the thermal instability of polyIL/[dema][TFAc] is related to back proton transfer from the cations of the IL to the anions, and volatilization of the reformed parent base. Another measure of the strength of proton transfer in the formation of protic ILs is given by the difference in the aqueous pK_a s of the precursor acid and base (ΔpK_a), which has been correlated with the vapour pressures of protic ionic liquids.⁴⁶ [dema][TFAc] has the lowest ΔpK_a of the three liquids, indicating that proton transfer from the parent acid to base is least complete in this IL, and making it the most thermally unstable.

Differential scanning calorimetry (DSC) of [dema][TfO], polyIL, polyIL/[dema][TfO], and polyIL/[dema][TFAc] membranes did not reveal any characteristic phase transitions in the range -20 °C to 190 °C. When heated to 250 °C, polyIm showed an endothermic peak at 220 °C, although no further transitions were observed when cooling down to 25 °C in the final cycle. This is correlated with the thermal instability of the polyIm membrane, as revealed using TGA (Figure 2A). By contrast, DSC of polyIL/[dema][Tf₂N] (Figure 2D) showed an endothermic peak on the heating cycle at 11 °C and an exothermic peak at -7 °C during the cooling cycling. These features

are related to melting and crystallization of [dema][Tf₂N], which appeared on the DSC traces at 13.5 °C and -0.7 °C respectively.

To investigate the spatial distribution of the ILs in the various GPEs, confocal Raman microscopy was used (Figure 3A and Figures S8-12 in the SI). The mean Raman spectrum extracted from lateral *xy* maps of the membrane surfaces (scanning a 225 × 225 μm area in either 5 or 10 μm steps) represents a clear superposition of the individual component spectra, with no significant shifting in the position or relative intensity of any of the peaks in the mean spectra, with respect to the component spectra, observed (see Tables S3 and S4 in the SI for spectral assignments). Surface and depth mapping of the polyIL/[dema][TfO] membrane indicated that there was only subtle variation in the [dema][TfO] content with respect to the polyIL host within the mapped areas (Figure 3B and S8), with the IL present at all locations. The average IL/PIL ratio in Figure 3B agrees with that ratio determined gravimetrically (Table S2). Similar behaviour was observed during analysis of polyIm/[dema][TfO] (Figure 3B and S9), polyIL/[dema][TFAc] (Figure S10), polyIL/[dema][Tf₂N] (Figure S11) and polyIL/[dema][TfO]-3D (Figure S12 and discussed further below), indicating that the distribution of the ILs throughout the membranes was not affected significantly by the charge on the polymer backbone, the nature of the IL anion, or the method of film fabrication. Interestingly, addition of 5 wt.% of a second polyIL, [PDADMA][Tf₂N], to form a polyIL/[PDADMA][Tf₂N]/[dema][TfO] composite resulted in a more pronounced change in the distribution of the IL upon depth profiling. Using a least squares regression analysis (Figure S14) we observed that the mobile [dema][TfO] phase strongly preferentially associates with the [PDADMA][Tf₂N] dopant, which itself appears to phase separate from the host [BVBIIm][Tf₂N] matrix (presumably as a result of the different hydrophobicities of the [BVBIIm] and [PDADMA]

cations in each polyIL). This suggests that the PDADMA-doped polyIL may be forming a semi-interpenetrating polymer network, a phenomena which has previously been explored as a strategy to tailor the physicochemical properties of GPEs for energy applications.^{47[}

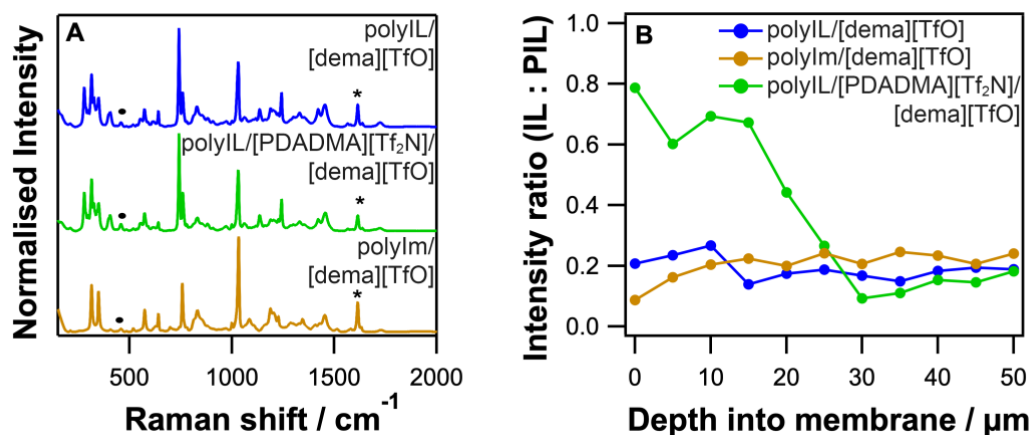


Figure 3. (A) Mean Raman spectra extracted from lateral top surface maps of polyIL/[dema][TfO] (blue), polyIm/[dema][TfO] (brown) and polyIL/[PDADMA][Tf₂N] / [dema][TfO] (green) membranes. The presence of [PDADMA][Tf₂N] in polyIL/[PDADMA][Tf₂N]/[dema][TfO] could not be confirmed by Raman spectroscopy and indicates its concentration in the film is lower than the detection threshold of the instrument. (B) z profiles showing the IL/polyIL ratio, as the intensity (as-area) ratio of the peak within the range 440-475 cm⁻¹ (assigned to the CNC and NCC bending modes in the [dema]⁺ cation of [dema][TfO]) to the peak within the range 1595-1630 cm⁻¹

¹ (assigned to a C=C stretching vibration in the aromatic ring of the cationic polymer of polyIL). The spectra in A have been offset on the y-axis and normalised to the intensity of the spectral maximum for clarity.

The conductivity of the GPEs was investigated using AC-impedance spectroscopy at a range of temperatures. Graphs of $\log \sigma$ versus T^{-1} (Figures 4A and 4B) were non-linear over the temperature range studied, and were fitted using the Vogel-Tamman-Fulcher equation:

$$\sigma = \sigma_0 \exp \left(\frac{-B}{T - T_0} \right) \quad (1)$$

where B is a pseudo-activation energy for conduction, σ_0 is the theoretical conductivity at infinite temperature, T is the absolute temperature and T_0 is ideal vitreous transition temperature at which the segmental motion begins. The best-fit T_0 and B values (Table 2) are comparable to those reported in the literature for other polyIL membranes.⁴⁸ In each case, the conductivity of the polyIL membrane was significantly higher than that of the corresponding polyIm membrane (6 times higher in the case of polyIL/[dema][Tf₂N], which contains the same anions in the polyIL and dopant IL), demonstrating the advantage of using the charged polymeric hosts over that of the neutral host. σ_0 corresponds to the number of carrier ions in the electrolyte and is higher for the polyIL membranes than for the corresponding polyIm membranes, due to the higher ion density in the polyIL/IL materials. Notably, the highest σ_0 was observed for polyIL/[PDADMA][Tf₂N]/[dema][TfO] containing 5% [PDADMA][Tf₂N], due to the incorporation of additional charge carriers. The fits of the VTF equation to the [dema][TFAC]

doped membranes were very poor (not shown), presumably due to the incomplete proton transfer in this system.



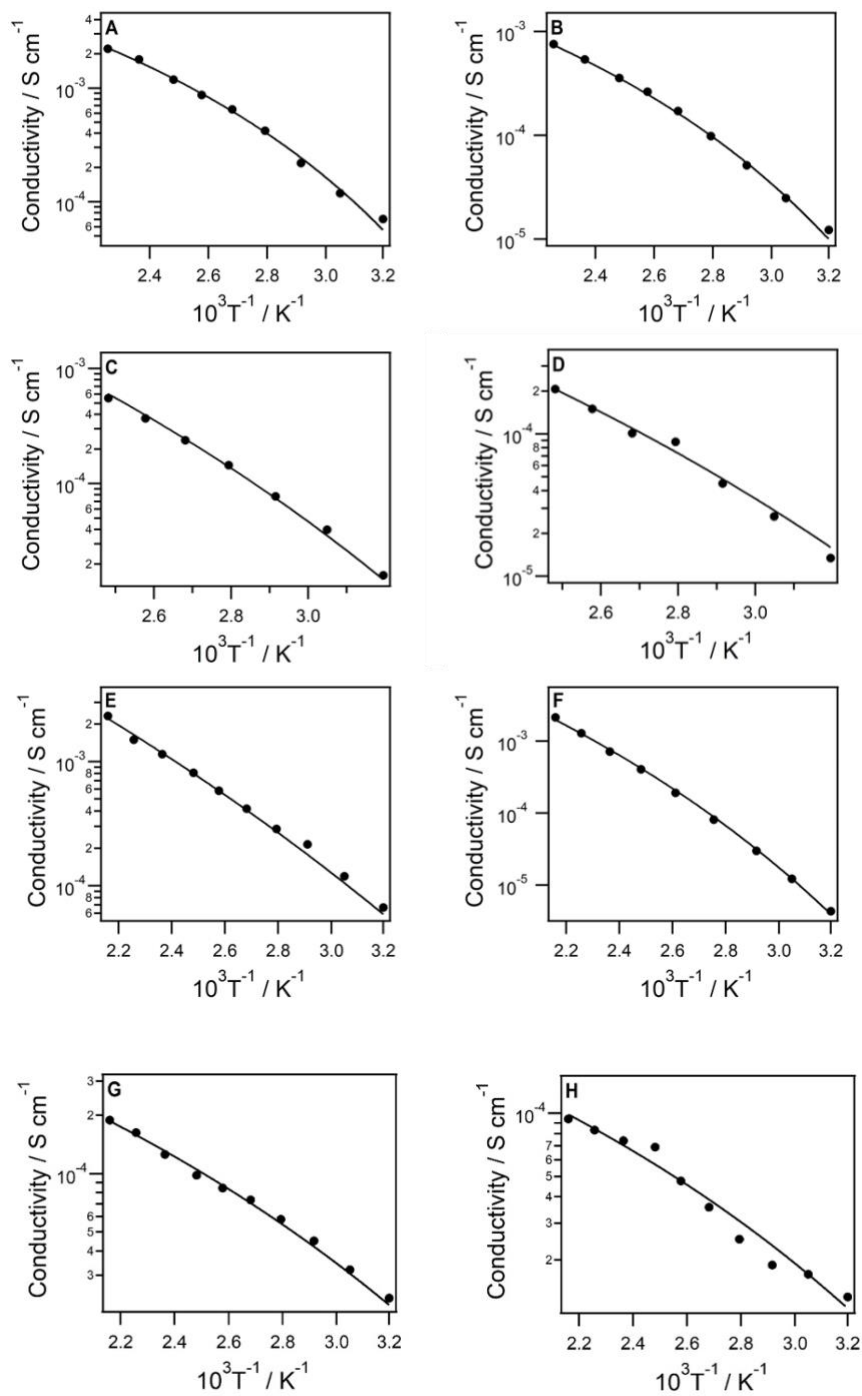


Figure 4. Plots of σ versus T^{-1} for (A) polyIL/[dema][Tf₂N], (B) polyIm/[dema][Tf₂N], (C) polyIL/[dema][TfO], (D) polyIm/[dema][TfO], (E) polyIL/[PDADMA][Tf₂N]/[dema][TfO], (F) polyIL/[dema][TfO]-3D, (G) polyIL/[dema][TFac], and (H) polyIm/[dema][TFac]. Black lines show are the best fits to Equation 1 and the best-fit parameters are in Table 2.

Table 2. Conductivities of GPE membranes.

Sample	T_0 / K	σ / S cm ⁻¹	B / K	σ at 40 °C / S cm ⁻¹
polyIL/[dema][Tf ₂ N]	204	0.0496	740	7.0×10^{-5}
polyIm/[dema][Tf ₂ N]	201	0.0304	896	1.2×10^{-5}
polyIL/[dema][TfO]	152	0.461	1670	3.4×10^{-5}
polyIm/[dema][TfO]	142	0.0265	1270	1.2×10^{-5}
polyIL/[PDADMA][Tf ₂ N] /[dema][TfO]	101	0.375	1860	6.7×10^{-5}
polyIL/[dema][TfO]-3D	164	0.950	1850	4.3×10^{-6}
polyIL/[dema][TFAc]	140	0.00230	816	2.3×10^{-5}
polyIm/[dema][TFAc]	150	0.00100	726	1.3×10^{-5}

Finally, we tested whether 3D printing could be used to print a polyIL/IL membrane. This technique is becoming increasingly common as a relatively accessible and cost-effective method to rapidly fabricate and prototype bespoke films, objects and devices.^{49,50} PolyILs are particularly well suited to the technique as monomers which are liquid at room temperature (such as those explored here) can easily be combined with existing commercially available printers, and interest in 3D-printable polyILs for catalytic, sensing, separation and energy applications has increased substantially over the past few years.⁵¹ Using the parameters described in the SI, 13 mm × 12 mm × 0.7 mm pieces of polyIL/[dema][TfO] were fabricated. Figure 5A shows a comparison of the 3D-

printed membrane and the non-3D printed analogue. The 3D-printed membrane was approximately 700 μm thick, which is notably thicker than the other GPEs which were about 100- μm thick. This greater thickness was probably the cause of the greater colouring of the 3D printed membranes compared to the apparently colourless polyIL/[dema][TfO] GPEs. There were also some small bubbles visible in the 3D printed membranes, due to trapping of air

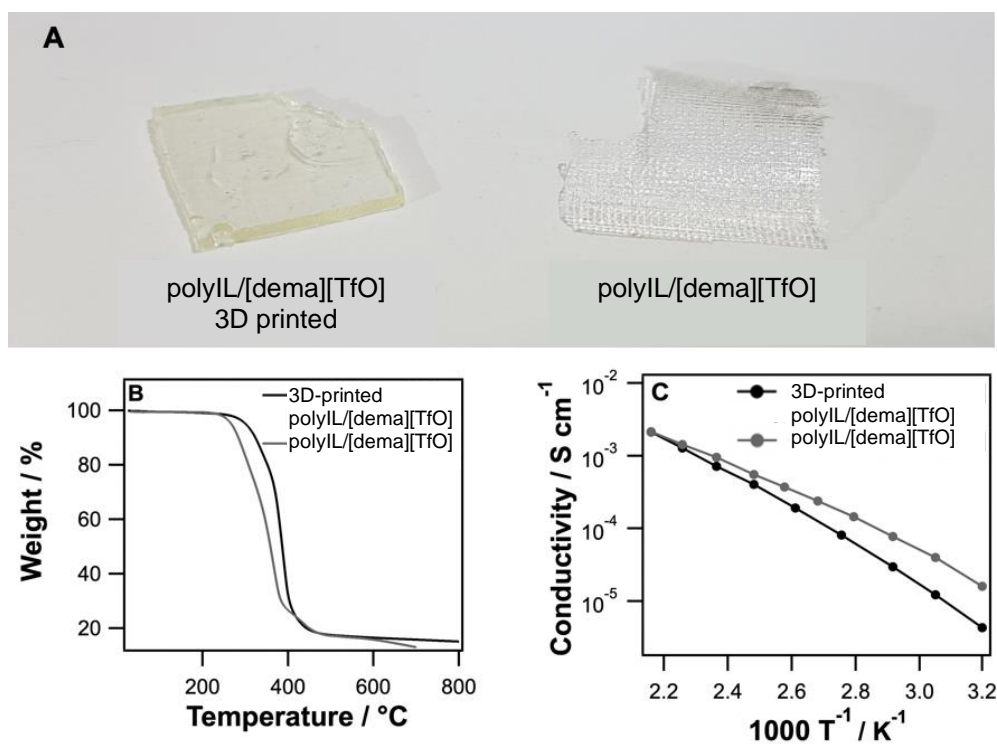


Figure 5. (A) Photographs of the polyIL/[dema][TfO] and 3D-printed polyIL/[dema][TfO] membranes. (B) TGA curves of the polyIL/[dema][TfO] (gray line) and 3D-printed polyIL/[dema][TfO] (black line) membranes. (C) Plots of conductivity vs. T^{-1} for polyIL/[dema][TfO] (gray line) and 3D-printed (black line) polyIL/[dema][TfO].

within the viscous monomer solution as the printer build plate moved up and down during printing. No holes that traversed the complete thickness of the printed piece were detected by optical microscopy. Polymerisation of the polyIL was confirmed by the absence of an infrared feature at approximately 1630 cm^{-1} in the FTIR spectrum of the printed piece.

It is also important to note that optimising the formulation of 3D-printable polyILs to yield satisfactory print quality whilst preserving the fundamental properties of the GPE is not necessarily trivial. For instance, while TGA analysis of the 3D printed membrane showed a lower rate of mass loss and greater residual mass than the polyIL/[dema][TfO] GPE (perhaps due to slower diffusion of IL from within the membrane) (Figure 5B), the conductivity of the 3D printed membrane was lower than that of polyIL/[dema][TfO] at low temperatures, though the membranes were equally conductive at elevated temperature (Figure 5C). Finally confocal Raman microscopy was used to examine the distribution of the IL throughout the membrane (Figure S12) and the distribution of [dema][TfO] throughout the membrane was more homogeneous than for the polyIL/[dema][TfO] membrane, demonstrating the opportunities offered by additive-manufacturing processes for the fabrication of polyIL/IL GPEs. Note that the additive manufacturing process could be optimised further in future by tuning of the composition of the monomer-containing formulation, reducing its environmental impact by recycling unused reagents during the printing process,⁵² or by using another 3D printing technique, such as inkjet printing, which could offer finer control over the thickness of the membranes.⁵³

Conclusions

In this work we have compared poly(ionic liquid)/ionic liquid GPEs (based on 1-butyl-3-(4-vinylbenzyl)imidazolium bis(trifluoromethanesulfonyl)imide as the host polymer and ammonium-based protic ionic as the trapped liquid component) with “conventional” polymer/ionic liquid GPEs (based on 1-(4-vinylbenzyl)imidazole as the host polymer) in terms of their thermal stability, distribution of ionic liquid, and conductivity. Raman spectroscopy was used to investigate the distribution of the trapped liquids within the membranes. The ionic-liquid components were evenly spread throughout the membranes except when [PDADMA][Tf₂N] was added to the poly(ionic liquid) GPE. This insight could provide a means to control the spatial distribution of ionic liquids within GPEs by fine tuning the starting preparation to drive selective phase separation within the polymerizing membrane. Despite the relatively high thermal stability of the ionic-liquid dopants, their incorporation into the ionic and neutral polymers resulted in a decrease in thermal stability of the resulting GPE. However, the poly(ionic liquid)/ionic liquid GPEs were more conductive than those based on the neutral host, demonstrating that use of the charged host frameworks results in a trade-off between achieving higher conductivities, but at the cost of lower thermal stabilities. Finally, we demonstrated that poly(ionic liquid) GPE membranes can be made using a 3D printing technique, which aided distribution of the ionic liquid throughout the formed piece, potentially offering new opportunities for the bespoke manufacture of electrolyte membranes for a range of applications.

Acknowledgements

We thank the EPSRC for funding through grant EP/P002382/1 and the University of Nottingham for support through the Beacon of Excellence in Propulsion Futures.

Supporting Information

Additional experimental details and characterization data. This information is available free of charge at

References

- [1] Berthod, A.; Ruiz-Angel, M.; Carda-Broch, S. Ionic Liquids in Separation Techniques. *J. Chromatogr. A* **2008**, *1184*, 6–18.
- [2] Silvester, D. S. Recent Advances in the Use of Ionic Liquids for Electrochemical Sensing. *Analyst* **2011**, *136*, 4871–4882.
- [3] MacFarlane, D. R.; Tachikawa, N.; Forsyth, M.; Pringle, J. M.; Howlett, P. C.; Elliott, G. D.; Davis, J. H.; Watanabe, M.; Simon, P.; Angell, C. A. Energy Applications of Ionic Liquids. *Energy Environ. Sci.* **2014**, *7*, 232–250.
- [4] van Rantwijk, F.; Sheldon, R. A. Biocatalysis in Ionic Liquids. *Chem. Rev.* **2007**, *107*, 2757–2785.
- [5] Nese, C.; Unterreiner, A. N. Photochemical Processes in Ionic Liquids on Ultrafast Timescales. *Phys. Chem. Chem. Phys.* **2010**, *12*, 1698–1708.
- [6] Ye, Y.-S.; Rick, J.; Hwang, B.-J. Ionic Liquid Polymer Electrolytes. *J. Mater. Chem. A* **2013**,

1, 2719–2743.

- [7] Thiemann, S.; Sachnov, S. J.; Pettersson, F.; Bollstrom, R.; Osterbacka, R.; Wasserscheid, P.; Zaumseil, J. Cellulose-Based Ionogels for Paper Electronics. *Adv. Funct. Mater.* **2014**, *24*, 625–634.
- [8] Curto, V. F.; Fay, C.; Coyle, S.; Byrne, R.; O'Toole, C.; Barry, C.; Hughes, S.; Moyna, N.; Diamond, D.; Benito-Lopez, F. Real-Time Sweat pH Monitoring Based on a Wearable Chemical Barcode Micro-Fluidic Platform Incorporating Ionic Liquids. *Sens. Actuators B* **2012**, *171*, 1327–1334.
- [9] Fdz De Anastro, A.; Lago, N.; Berlanga, C.; Galcerán, M.; Hilder, M.; Forsyth, M.; Mecerreyes, D. Poly(Ionic Liquid) Ionogel Membranes for All Solid-State Rechargeable Sodium Battery. *J. Memb. Sci.* **2019**, *582*, 435–441.
- [10] Izák, P.; Hovorka, Š.; Bartovský, T.; Bartovská, L.; Crespo, J. G. Swelling of Polymeric Membranes in Room Temperature Ionic Liquids. *J. Memb. Sci.* **2007**, *296*, 131–138.
- [11] Samir, M.; Alloin, F.; Dufresne, A. Review of Recent Research into Cellulosic Whiskers, Their Properties and Their Application in Nanocomposite Field. *Biomacromolecules* **2005**, *6*, 612–626.
- [12] Susan, M. A. B. H.; Kaneko, T.; Noda, A.; Watanabe, M. Ion Gels Prepared by in Situ Radical Polymerization of Vinyl Monomers in an Ionic Liquid and Their Characterization as Polymer Electrolytes. *J. Am. Chem. Soc.* **2005**, *127*, 4976–4983.
- [13] Xie, M.; Li, S.; Huang, Y.; Wang, Z.; Jiang, Y.; Wang, M.; Wu, F.; Chen, R. An Ionic Liquid/Poly(Vinylidene Fluoride-Co-Hexafluoropropylene) Gel-Polymer Electrolyte with a Compatible Interface for Sodium-Based Batteries. *ChemElectroChem* **2019**, *6*, 2423–

2429.

- [14] Yang, Y.; Gao, H.; Zheng, L. Anhydrous Proton Exchange Membranes at Elevated Temperatures: Effect of Protic Ionic Liquids and Crosslinker on Proton Conductivity. *RSC Adv.* **2015**, *5*, 17683–17689.
- [15] Langevin, D.; Nguyen, Q. T.; Marais, S.; Karademir, S.; Sanchez, J.-Y.; Iojoiu, C.; Martinez, M.; Mercier, R.; Judeinstein, P.; Chappey, C. High-Temperature Ionic-Conducting Material: Advanced Structure and Improved Performance. *J. Phys. Chem. C* **2013**, *117*, 15552–15561.
- [16] Salamone, J. C.; Israel, C. S.; Taylor, P. Snider, B. Polyvinylimidazolium Salts of Varying Hydrophilic-hydrophobic Character. *J. Polym. Sci. Polym. Symp.* **1974**, *45*, 65–73.
- [17] Hiroyuki, O. Design of Ion Conductive Polymers Based on Ionic Liquids. *Macromol. Symp.* **2007**, *249–250*, 551–556.
- [18] Zhang, S. Y.; Zhuang, Q.; Zhang, M.; Wang, H.; Gao, Z.; Sun, J. K.; Yuan, J., Poly(ionic liquid) Composites. *Chem. Soc. Rev.*, **2020**, *49*, 1726-1755.
- [19] Yuan, J.; Mecerreyes, D.; Antonietti, M. Poly(Ionic Liquid)s: An Update. *Prog. Polym. Sci.* **2013**, *38*, 1009–1036.
- [20] Forsyth, M.; Porcarelli, L.; Wang, X.; Goujon, N.; Mecerreyes, D. Innovative Electrolytes Based on Ionic Liquids and Polymers for Next-Generation Solid-State Batteries. *Acc. Chem. Res.* **2019**, *52*, 686–694.
- [21] Carlisle, T. K.; McDanel, W. M.; Cowan, M. G.; Noble, R. D.; Gin, D. L. Vinyl-Functionalized Poly(Imidazolium)s: A Curable Polymer Platform for Cross-Linked Ionic Liquid Gel Synthesis. *Chem. Mater.* **2014**, *26*, 1294–1296.

- [22] Appetecchi, G. B.; Kim, G. T.; Montanino, M.; Carewska, M.; Marcilla, R.; Mecerreyes, D.; De Meazza, I. Ternary Polymer Electrolytes Containing Pyrrolidinium-Based Polymeric Ionic Liquids for Lithium Batteries. *J. Power Sources* **2010**, *195*, 3668–3675.
- [23] Díaz, M.; Ortiz, A.; Isik, M.; Mecerreyes, D.; Ortiz, I. Highly Conductive Electrolytes Based on Poly([HSO₃-BVIm][TfO])/[HSO₃-BMIm][TfO] Mixtures for Fuel Cell Applications. *Int. J. Hydrogen Energy* **2015**, *40*, 11294–11302.
- [24] Díaz, M.; Ortiz, A.; Vilas, M.; Tojo, E.; Ortiz, I. Performance of PEMFC with New Polyvinyl-Ionic Liquids Based Membranes as Electrolytes. *Int. J. Hydrogen Energy* **2014**, *39*, 3970–3977.
- [25] Nair, J. R.; Colo, F.; Kazzazi, A.; Moreno, M.; Bresser, D.; Lin, R.; Bella, F.; Meligrana, G.; Fantini, S.; Simonetti, E.; Appetecchi, G. B.; Passerini, S; Gerbaldi, C. Room Temperature Ionic Liquid (RTIL)-Based Electrolyte Cocktails for Safe, High Working Potential Li-Based Polymer Batteries. *J. Power Sources* **2019**, *412*, 398–407.
- [26] Döbbelin, M.; Azcune, I.; Bedu, M.; de Luzuriaga, A.; Genua, A.; Jovanovski, V.; Cabañero, G.; Odriozola, I. Synthesis of Pyrrolidinium-Based Poly(Ionic Liquid) Electrolytes with Poly(Ethylene Glycol) Side Chains. *Chem. Mater.* **2012**, *24*, 1583–1590.
- [27] Nakajima, H.; Ohno, H. Preparation of Thermally Stable Polymer Electrolytes from Imidazolium-Type Ionic Liquid Derivatives. *Polymer* **2005**, *46*, 11499–11504.
- [28] Chen, X.; Zhao, J.; Zhang, J.; Qiu, L.; Xu, D.; Zhang, H.; Han, X.; Sun, B.; Fu, G.; Zhang, Y.; Yan, F. Bis-Imidazolium Based Poly(Ionic Liquid) Electrolytes for Quasi-Solid-State Dye-Sensitized Solar Cells. *J. Mater. Chem.* **2012**, *22*, 18018–18024.
- [29] Yasuda, T.; Watanabe, M. Protic Ionic Liquids: Fuel Cell Applications. *MRS Bulletin* **2013**,

38, 560-566.

- [30] Greaves, T. L.; Drummond, C. J. Protic Ionic Liquids: Evolving Structure-Property Relationships and Expanding Applications. *Chem. Rev.* **2015**, *115*, 11379-11448.
- [31] Ye, H.; Huang, J.; Xu, J. J.; Kodiweera, N. K. A. C.; Jayakody, J. R. P.; Greenbaum, S. G. New Membranes based on Ionic Liquids for PEM Fuel Cells at Elevated Temperatures. *J. Power Sources* **2008**, *178*, 651-660.
- [32] Fatyeyeva, K.; Rogalsky, S.; Makhno, S.; Tarasyuk, O.; Puente, J. A. S.; Marais, S. Polyimide/Ionic Liquid Composite Membranes for Middle and High Temperature Fuel Cell Application: Water Sorption Behavior and Proton Conductivity. *Membranes* **2020**, *10*, 82.
- [33] Lee, S. -Y.; Ogawa, A.; Kanno, M.; Nakamoto, H.; Yasuda, T.; Watanabe, M. Nonhumidified Intermediate Temperature Fuel Cells Using Protic Ionic Liquids, *J. Am. Chem. Soc.* **2010**, *132*, 9764-9773.
- [34] Wales, D. J.; Cao, Q.; Kastner, K.; Karjalainen, E.; Newton, G. N.; Sans, V. 3D-Printable Photochromic Molecular Materials for Reversible Information Storage. *Adv. Mater.* **2018**, *30*, 1-7.
- [35] Goodwin, S. E.; Smith, D.; Gibson, J.; Jones, R. G.; Walsh, D. A. Electroanalysis of Neutral Precursors in Protic Ionic Liquids and Synthesis of High-Ionicity Ionic Liquids. *Langmuir* **2017**, *33*, 8436-8446.
- [36] Overberger, C. G.; Vorchheimer, N. Imidazole-Containing Polymers. Synthesis and Polymerization of the Monomer 4(5)-Vinylimidazole. *J. Am. Chem. Soc.* **1963**, *85*, 951-955.

- [37] Pretsch, E.; Bühlmann, P.; Badertscher, M. *Structure Determination of Organic Compounds*; Springer-Verlag, Berlin Heidelberg, 2009.
- [38] Safna Hussein; K. P. Thayyil, M. S.; Deshpande, S. K.; Jinatha, T. V.; Kolte, J. Development of Ion Conducting Ionic Liquid-Based Gel Polymer Electrolyte Membrane PMMA/BMPyr.TFSI - With Improved Electrical, Optical, Thermal and Structural Properties. *Solid State Ionics* **2017**, *310*, 166–175.
- [39] Wang, X.; Zhu, H.; Girard, G. A.; Yunis, R.; MacFarlane, D. R.; Mecerreyes, D.; Bhattacharyya, A. J.; Howlett, P. C.; Forsyth, M. Preparation and Characterization of Gel Polymer Electrolytes Using Poly(Ionic Liquids) and High Lithium Salt Concentration Ionic Liquids. *J. Mater. Chem. A* **2017**, *5*, 23844–23852.
- [40] Chi, W. S.; Hong, S. U.; Jung, B.; Kang, S. W.; Kang, Y. S.; Kim, J. H. Synthesis, Structure and Gas Permeation of Polymerized Ionic Liquid Graft Copolymer Membranes. *J. Memb. Sci.* **2013**, *443*, 54–61.
- [41] Wang, X.; Jin, M.; Li, Y.; Zhao, L. The Influence of Various Ionic Liquids on the Properties of SPEEK Membrane Doped with Mesoporous Silica. *Electrochim. Acta* **2017**, *257*, 290–300.
- [42] Li, Y.; Zhang, M.; Wang, X.; Li, Z.; Zhao, L. Anhydrous Conducting Composite Membranes Composed of SPEEK/Silica/Ionic Liquids for High-Temperature Proton Exchange. *Electrochim. Acta* **2016**, *222*, 1308–1315.
- [43] Switzer, E. E.; Zeller, R.; Chen, Q.; Sieradzki, K.; Buttry, D. A.; Friesen, C. Oxygen Reduction Reaction in Ionic Liquids: The Addition of Protic Species. *J. Phys. Chem. C* **2013**, *117*, 8683–8690.

- [44] Millan, D.; Rojas, M.; Santos, J. G.; Morales, J.; Isaacs, M.; Diaz, C.; Pavez, P. Toward a pK_a Scale of N-base Amines in Ionic Liquids. *J. Phys. Chem. B* **2014**, *118*, 4412–4418.
- [45] Davidowski, S. K.; Thompson, F.; Huang, W.; Hasani, M.; Amin, S. A.; Angell, C. A.; Yarger, J. L. NMR Characterization of Ionicity and Transport Properties for a Series of Diethylmethylamine Based Protic Ionic Liquids. *J. Phys. Chem. B* **2016**, *120*, 4279–4285.
- [46] Yoshizawa, M.; Xu, W.; Angell, C. A. Ionic Liquids by Proton Transfer: Vapor Pressure, Conductivity, and the Relevance of ΔpK_a from Aqueous Solutions. *J. Am. Chem. Soc.* **2003**, *125*, 15411–15419.
- [47] Shaplov, A. S.; Ponkratov, D. O.; Vlasov, P. S.; Lozinskaya, E. I.; Gumileva, L. V.; Surcin, C.; Morcrette, M.; Armand, M.; Aubert, P. -H.; Vidald, F.; Vygodskii, Y. S.; *J. Mater. Chem. A*. **2015**, *3*, 2188-2198.
- [48] Green, M. D.; Wang, D.; Hemp, S. T.; Choi, J. H.; Winey, K. I.; Heflin, J. R.; Long, T. E. Synthesis of Imidazolium ABA Triblock Copolymers for Electromechanical Transducers. *Polymer* **2012**, *53*, 3677–3686.
- [49] Capel, A. J.; Rimington, R. P.; Lewis, M. P.; Christie, S. D. R. 3D Printing for Chemical, Pharmaceutical and Biological Applications. *Nat. Rev. Chem.* **2018**, *2*, 422-436.
- [50] Browne, M. P.; Redondo, E.; Pumera, M. 3D Printing for Electrochemical Energy Applications. *Chem. Rev.* **2020**, *120*, 2783–2810.
- [51] Nulwala, H.; Mirjafari, A.; Zhou, X. Ionic Liquids and Poly(ionic liquid)s for 3D Printing – A Focused Mini-review. *Eur. Polym. J.* **2018**, *108*, 390-398.
- [52] Maciel, V.; Wales, D.; Seferin, M.; Ugaya, C.; Sans, V. State-of-the-Art and Limitations in the Life Cycle Assessment of Ionic Liquids. *J. Clean. Prod.* **2019**, *217*, 844–858.

- [53] Karjalainen, E.; Wales, D. J.; Gunasekera, D. H. A. T.; Dupont, J.; Licence, P.; Wildman, R. D.; Sans, V. Tunable Ionic Control of Polymeric Films for Inkjet Based 3D Printing. *ACS Sust. Chem. Eng.* **2018**, *6*, 3984–3991

TOC Graphic

